Journal of Sound and Vibration (2000) **237**(5), 875–900
doi:10.1006/jsvi.2000.3148, available online at http://www.idealibrary.com on IDEAL®

NON-LINEAR COUPLED TRANSVERSE AND AXIAL VIBRATION OF A COMPLIANT STRUCTURE, PART 2: FORCED VIBRATION

S. M. Han and H. Benaroya

Mechanical and Aerospace Engineering, Rutgers, the State University of New Jersey, Piscataway, NJ 08854, *USA*

(*Received* 28 *October* 1999, *and in final form* 5 *June* 2000)

Responses of a beam undergoing both axial and transverse vibration are studied when the beam is subjected to transverse forces. The beam is supported by a torsional spring at the base and has a point mass at the free end. This is a simplified model of a complaint offshore structure. It is assumed that the environmental forces are due to waves and current. The semi-empirical Morison equation is used to model the fluid forces. Waves in this case are assumed to be random and their heights follow the Pierson–Moskowitz spectrum. Borgman's method is used to obtain the wave height from the Pierson-Moskowitz spectrum, and the wave velocities and the accelerations are obtained from the wave height using the Airy linear wave theory. The wave velocities and accelerations are then used in the Morison equation to form the fluid forcing function. As a preliminary study, the harmonic force is used to model the fluid force. When the deterministic harmonic force at various frequencies is applied, subharmonic resonances of order 1/2 are observed. Parametric studies of random forcing are performed by varying current velocity and significant wave height.

1. INTRODUCTION

In Part 1 of this work [1], we investigated the free response in vacua and the damped free response in water of a beam as shown in Figure 1. Previously, we used the coupled non-linear beam model that included both axial and transverse motion to obtain the response. The equations of motion were solved numerically using the finite difference approach. The solutions were in terms of transverse and axial displacements, the displacements in the x and y directions from the reference configuration as shown in Figure 2. It was found that the fundamental frequency of the axial motion is twice as that of the transverse motion. This frequency is induced geometrically. It was shown that the fundamental frequencies and the contribution of high-frequency effects varied with initial conditions. When damped responses were considered, we showed that the Morison force can only affect the axial motion through transverse motion.

The purpose of this study is to investigate forced responses of a beam with the same configuration using the non-linear coupled beam model. In an ocean environment, offshore structures may experience forces due to waves, current, and wind. Here, we ignore the wind force since the part that is subjected to wind force is small compared with the rest of the structure.

The fluid force exerted by the current and waves include drag, added mass, and inertia forces which act in the xy plane as shown in Figure 1. There is also a force arising from shedding vortices which causes the beam to vibrate in the xz plane. There exists a wave

0022-460X/00/450875 + 26 $35.00/0

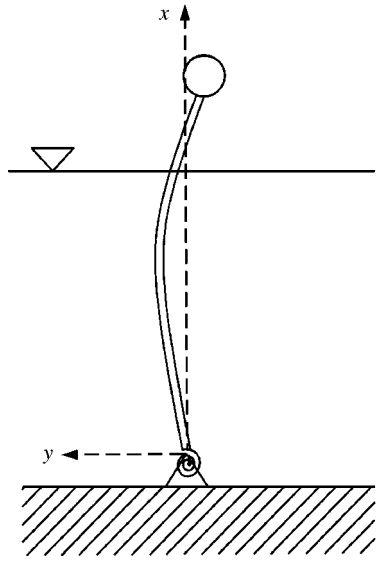

Figure 1. Schematic of an offshore structure.

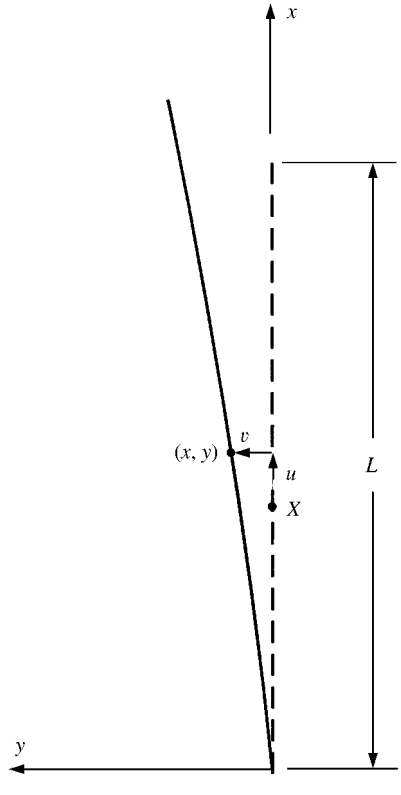

Figure 2. Reference and current midplane configurations of the beam.

slamming force, which is an impulsive force by the waves on the structure above the water level. Here, we do not consider either the vortex shedding force nor the wave slamming force. The drag, added mass, and inertia forces are modelled using the Morison equation. The Morison equation requires coefficients that are determined by experiments.

The current velocity can be assumed to be constant with time. On the other hand, the wave velocities and accelerations are oscillatory. Here, we consider random waves; therefore, a broadband of frequencies are present in the waves.

As a preliminary study, we look at the responses when the structure is subjected to a force with a single frequency. The forcing frequency is varied so that non-linear properties such as subharmonics and superharmonics can be shown. When the random Morison force is used, we first look at the effect of the varying current velocity without waves, and we look at the effect of varying significant wave height.

We hope to see in the response the non-linear characteristics such as subharmonic resonance.

2. MATHEMATICAL MODEL

2.1. STRUCTURE

In the first part of this work, we derived the governing equation of motion given by [1]

$$\rho A_o \ddot{u} - (EA_o(u' + \tfrac{1}{2}v'^2))' = p,$$

$$\rho A_o \ddot{v} - (EA_o(u' + \tfrac{1}{2}v'^2)v')' - (\rho I_o \ddot{v}')' + (EI_o v'')'' = f \tag{1}$$

with corresponding boundary conditions given by

$$u(0, t) = 0,\ [EA_o(u' + \tfrac{1}{2}v'^2) + M_p\ddot{u}]|_{L,t} = 0,$$

$$v(0, t) = 0, \quad kv' - EI_o v''|_{0,t} = 0,$$

$$[(EI_o v'')' - \rho I_o \ddot{v}' - EA_o(u' + \tfrac{1}{2}v'^2)v' - M_p\ddot{v}]|_{L,t} = 0, \quad EI_o v''(L, t) = 0, \tag{2}$$

where ρ is the density of the structure. A_o is the cross-sectional area, E is Young's modulus, I_o is the area moment of inertia about the neutral axis, M_p is the point mass, k is the torsional spring constant, and L is the length of the undeformed beam.

Note that the axial displacement u, transverse displacement v, axial distributed load p, and the transverse distributed load f are functions of both X and t. The prime and dot notations are used for spatial and time derivatives respectively. The axial and transverse displacements are measured from the reference configuration as shown in Figure 2.

In all cases, the distributed axial force $p(X, t)$ is due to gravity and buoyancy and is given by

$$p(X, t) = -\rho g A_o + \rho_f g A_f \quad \text{for } 0 < X \leqslant d$$

$$-\rho g A_o \quad \text{for } d < X < L, \tag{3}$$

where ρ_f is the density of the surrounding fluid, g is the gravitational acceleration, A_f is the cross-section of the displaced volume πr_{outer}^2, and d is the water depth.

2.2. FLUID FORCING

2.2.1. *The Morison equation*

In the first part of this study, we used the Morison force to simulate the transverse fluid force in still water. The expression is given by [2]

$$f(X,t) = -C_A\rho_f A_f\ddot{R}^n + C_M\rho_f A_f\dot{U}^n + C_D\rho_f r_{outer}V_{rel}^n|V_{rel}^n|, \tag{4}$$

where $\ddot{R}$ is the acceleration of the beam, $\dot{U}$ is the acceleration of the fluid, and V_{rel} is the relative velocity of fluid with respect to the structure. The superscript n is used to indicate that they are normal components (normal to the structure). C_A is the added mass coefficient, C_D is the drag coefficient, and C_M is the inertia coefficient. The first term in equation (4) is the added mass term, the second is the inertial term, and the third is the drag term.

In vectorial form, we can write the velocity and the acceleration of the structure as

$$\dot{\mathbf{R}} = \dot{u}\mathbf{i} + \dot{v}\mathbf{j}, \qquad \ddot{\mathbf{R}} = \ddot{u}\mathbf{i} + \ddot{v}\mathbf{j}. \tag{5}$$

The relative velocity of the fluid with respect to the structure is given by

$$\mathbf{V}_{rel} = (w_x - \dot{u})\mathbf{i} + (w_y + U_c - \dot{v})\mathbf{j}, \tag{6}$$

where w_y and w_y are wave velocities in x and y directions respectively. Note that we assumed that the current flows in the y direction only.

The normal components can be obtained by performing the double cross-products

$$\ddot{R}^n = |\mathbf{1}\times\ddot{\mathbf{R}}\times\mathbf{1}|, \qquad V_{rel}^n = |\mathbf{1}\times\mathbf{V}_{rel}\times\mathbf{1}|, \tag{7}$$

where the tangent vector $\mathbf{1}$ (to the structure) is given by

$$\mathbf{1} = \mathbf{i} + v'\mathbf{j}. \tag{8}$$

The double cross-product, $\mathbf{1}\times\mathbf{Q}\times\mathbf{1}$, produces a vector that is normal to $\mathbf{1}$ and is on the plane defined by $\mathbf{1}$ and $\mathbf{Q}$.

Note that the small angle assumption is used to approximate the sine of the rotation by the slope and cosine of the rotation by unity. The resulting normal vectors are given by

$$\begin{aligned}\ddot{R}^n &= -\ddot{u}v' + \ddot{v},\\ V_{rel}^n &= (-w_x + \dot{u})v' + (w_y + U_c - \dot{v})\\ &= w_y - w_x v' + \dot{u}v' - \dot{v} + U_c.\end{aligned} \tag{9}$$

Finally, the transverse force is given by

$$\begin{aligned}f(X,t) = &-C_A\rho_f A_f(-\ddot{u}v' + \ddot{v}) + C_M\rho_f A_f(\dot{w}_y - \dot{w}_x v')\\ &+ C_D\rho_f r_{outer}(w_y - w_x v' + \dot{u}v' - \dot{v} + U_c)|w_y - w_x v' + \dot{u}v' - \dot{v} + U_c|.\end{aligned} \tag{10}$$

2.2.2. *Current and random waves*

According to Isaacson [3], the current velocity in an ocean environment consists of three components: tidal components U_{tide}, a low-frequency component related to long-term circulation $U_{circulation}$, and wind-induced drift current U_{drift}. They are measured at the water surface (at $X = d$). It is assumed that the current velocity has only a horizontal component.

The current velocity is then given by

$$U_c(X) = (U_{tide}(d) + U_{circulation}(d))\left(\frac{X}{d}\right)^{1/7} + U_{drift}(d)\left(\frac{X - d + d_o}{d_o}\right), \tag{11}$$

where d_o is the smaller of the depth of the thermocline or 50 m. In a laboratory setting, we can assume that the current velocity is constant with both time and depth without deviating too much from reality.

In the previous section, we formulated the fluid force using the Morison equation. The Morison equation requires a knowledge of wave and current velocities. The wave velocities are more involved since they are oscillatory at random frequencies by nature.

In order to obtain the wave velocities and accelerations, we use the Airy linear wave theory and the Pierson–Moskowitz spectrum for the wave height. From the Airy linear wave theory, the wave height is given by

$$\eta(y, t) = A\cos(ky - \omega t), \tag{12}$$

where A is the amplitude of the wave as shown in Figure 3.

The corresponding wave velocities are given by

$$w_y(x, y, t) = A\omega\frac{\cosh kx}{\sinh kd}\cos(ky - \omega t),$$

$$w_x(x, y, t) = A\omega\frac{\sinh kx}{\sinh kd}\sin(ky - \omega t) \tag{13}$$

and the dispersion relation is given by

$$\omega^2 = gk\tanh kd. \tag{14}$$

Note that the Airy wave theory assumes that the wave height is small compared to the wavelength or water depth [4].

The one-sided Pierson–Moskowitz spectrum is given by [4]

$$S(\omega) = \frac{0{\cdot}7795}{\omega^5}\,\mathrm{e}^{-(3{\cdot}12/H_s^2)\omega^{-4}} \quad (\mathrm{m}^2\mathrm{s}), \tag{15}$$

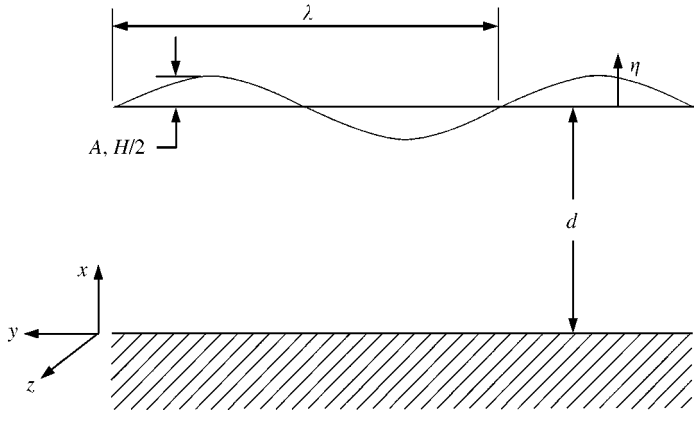

Figure 3. Waves.

where H_s is the significant wave height, which is the average of the height of the highest one-third of all waves [5]. Mathematically, it is four times the variance [4]. The frequency at which the power spectrum is maximum is given by

$$\omega_{peak} = \frac{1{\cdot}2568}{\sqrt{H_s}} \quad \text{(rad/s)}. \tag{16}$$

The wave height is then given by [6]

$$\eta(y, t) = \int_0^\infty \cos(ky - \omega t)\sqrt{S(\omega)\,\mathrm{d}\omega}. \tag{17}$$

In order to carry out the integration, we used the method suggested by Borgman [7]. The integral is represented as a finite sum by dividing the power spectrum into N equal areas. After mathematical manipulations, the wave height is given by

$$\eta(y, t) = \frac{H_s}{4\sqrt{N}} \sum_{n=1}^{N} \cos(\bar{k}_n y - \bar{\omega}_n t), \tag{18}$$

where N is the number of intervals and $\bar{\omega}_n$ is the average value of the angular frequency at the nth interval. $\bar{k}_n$ is the wave number that corresponds to $\bar{\omega}_n$, and it is obtained using the dispersion relationship in equation (14). Using the Airy linear wave theory, the wave velocities are given by

$$w_y(x, y, t) = \frac{H_s}{4\sqrt{N}} \sum_{n=1}^{N} \bar{\omega}_n \frac{\cosh \bar{k}_n x}{\sinh \bar{k}_n d} \cos(\bar{k}_n y - \bar{\omega}_n t),$$

$$w_x(x, y, t) = \frac{H_s}{4\sqrt{N}} \sum_{n=1}^{N} \bar{\omega}_n \frac{\sinh \bar{k}_n x}{\sinh \bar{k}_n d} \sin(\bar{k}_n y - \bar{\omega}_n t). \tag{19}$$

The wave accelerations are obtained by taking time derivatives. The wave velocities need to be evaluated at the beam location. That is, y is replaced by $v(X, t)$. Also, x needs to be replaced by $X + u(X, t)$ since we are using the Lagrangian formulation.

In order to determine the wave velocities, the only variable to be specified is the significant wave height.

3. RESULTS AND DISCUSSION

For numerical purposes, we consider a beam identical to that used in the first part of this study. The beam and the fluid properties are given in Tables 1 and 2.

The drag coefficient of 1 is a reasonable value for the Reynolds number of our flow [8]. For a long cylinder, the inertia coefficient approaches its theoretical value (the value for a uniformly accelerated flow) of 2, and the added mass coefficient related to the inertia coefficient by

$$C_A = C_M - 1 \tag{20}$$

approaches 1. We use these theoretical values for numerical purposes.

Here, we consider either zero initial conditions or initial displacements obtained from the physical configuration shown in Figure 4 with zero initial velocities.

TABLE 1

The beam properties

Beam properties	
Material	Aluminum
Young's modulus, E	73 GPa
Density, ρ	2770 kg/m^3
Point mass, M_p	0·236 kg
Torsional spring constant, k	38·8 N/m
Length, L	1·27 m
Outer radius, r_o	0·0127 m
Inner radius r_i	0·011 m

TABLE 2

The fluid properties

Fluid properties	
Density of water, ρ_f	999 kg/m^3
Water depth, d	1·05 m
Current velocity, U_c	0·12 m/s
Significant wave height, H_s	0·05–0·2 m
Added mass coefficient, C_A	1
Inertia coefficient, C_M	2
Drag coefficient, C_D	1
Re	2718·7

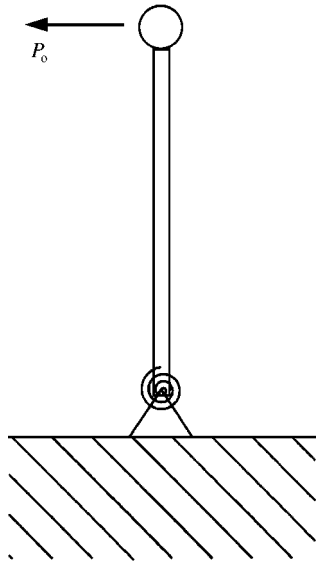

Figure 4. Initial configuration.

The point load is determined such that the end transverse deflection is 0·05 m. The expressions for the displacement are given in equation (21):

$$u(X,0) = -\frac{1}{2}\left(\frac{P_o}{EI}\right)^2\left(\frac{X^5}{20} - \frac{LX^4}{4} + \left(L^2 - \frac{EIL}{k}\right)\frac{X^3}{3} + \frac{EIL^2X^2}{k} + \left(\frac{EIL}{k}\right)^2 X\right),$$

$$v(X,0) = -\frac{P_o}{EI}\left(\frac{X^3}{6} - \frac{LX^2}{2} - \frac{EILX}{k}\right). \tag{21}$$

Note that these displacements are identical to the initial displacements IC_1 used in Part 1 of this study.

In free vibration, we found that the fundamental frequency of the transverse motion is 7·75 rad/s in vacua and 6·78 rad/s in still water.

Here, we apply two kinds of distributed transverse loads: a simple harmonic and a random force. The fluid force due to random waves has many frequency components. Therefore, it may be useful to consider a transverse load with single frequency first. The distributed axial load in equation (3) is used for all cases.

3.1. HARMONIC FORCING

Let us assume that the distributed transverse load is constant over the length of the beam and varies harmonically with time. That is

$$f(X,t) = \rho_f A_f \cos\omega_f t. \tag{22}$$

In order to obtain a reasonable deflection that is small enough such that the small angle assumption is valid, the coefficient of the harmonic function is chosen as $\rho_f A_f$.

3.1.1. *Subharmonics*

If we see a periodic response to a forcing frequency that is a multiple of the natural frequency, it is called a subharmonic response. Similarly, if we see a periodic response to a forcing frequency that is a fraction of the natural frequency, it is called a superharmonic or ultraharmonic response. In both cases, the system responds at the lower frequency of the two. That is, the system responds at the natural frequency for the subharmonics and at the forcing frequency for the superharmonics [9]. The superharmonics are called ordinary harmonics in the sense that the system response is at the input forcing frequency [10].

Subharmonics and superharmonics can be seen in both linear and non-linear systems. Those seen in linear systems are due to exact relations between the natural and forcing frequencies. That is, the forcing frequency has to be an exact multiple or an exact fraction of the natural frequency. Recall that there are two parts to the solution to the linear oscillator; the homogeneous and the particular solution. The homogeneous part oscillates at the natural frequency, and the particular part oscillates at the forcing frequency. The magnitude of the homogeneous part is determined exactly from initial conditions, the forcing frequency, and the amplitude of the force. The subharmonic state enters when the forcing frequency is twice the natural frequency, and the magnitude of the homogeneous solution is large compared to that of the particular solution. Similarly, the superharmonic state enters when the forcing frequency is half the natural frequency, and the magnitude of the homogeneous solution is small compared to that of the particular solution. Therefore, subharmonics and superharmonics may or may not appear depending on the

initial conditions and the amplitude of forcing when a suitable forcing frequency is set of each case.

Non-linear systems are slightly different in that the non-linearity of the system can generate stable harmonics that can appear for a range of forcing frequencies, instead of at exact values of forcing frequency. Again, subharmonics and superharmonics may or may not appear depending on the initial conditions and forcing amplitude.

The governing equations of motion (1) have second order non-linear terms. This indicates that the response may exhibit subharmonics of order 1/2 and super-harmonics of order 2. Therefore, we look for subharmonics for the forcing frequency near twice the natural frequency and superharmonics near half the natural frequency.

It has been observed that the subharmonics exist in offshore structures such as landing ships tanks (LST's) during mooring [11]. Here, let us only consider subharmonic responses.

The forcing frequency is varied from 2 to 18 at 2 rad/s increment. Figure 5 shows the transverse displacement when zero initial conditions are used. We notice that the response grows when the forcing frequency approaches the natural frequency (around 7·75–8·48 rad/s). The subharmonic state did not enter here. The subharmonic response can be seen only when the forcing frequency is 15·5 rad/s, as shown in Figure 6 where the system responds at half the input forcing frequency. This behavior is similar to what we see in the linear responses where an exact relationship between the natural and forcing frequency is required in order for the subharmonic state to enter.

On the other hand, the transverse displacement in Figure 7, obtained using the initial conditions given in equation (21), shows the subharmonic response for forcing frequencies that are not exactly twice the natural frequency. In Figures 7(g)–7(i), we observed that the system responds at the natural frequency when it is forced at a frequency close to twice the natural frequency. This is characteristic of a non-linear system.

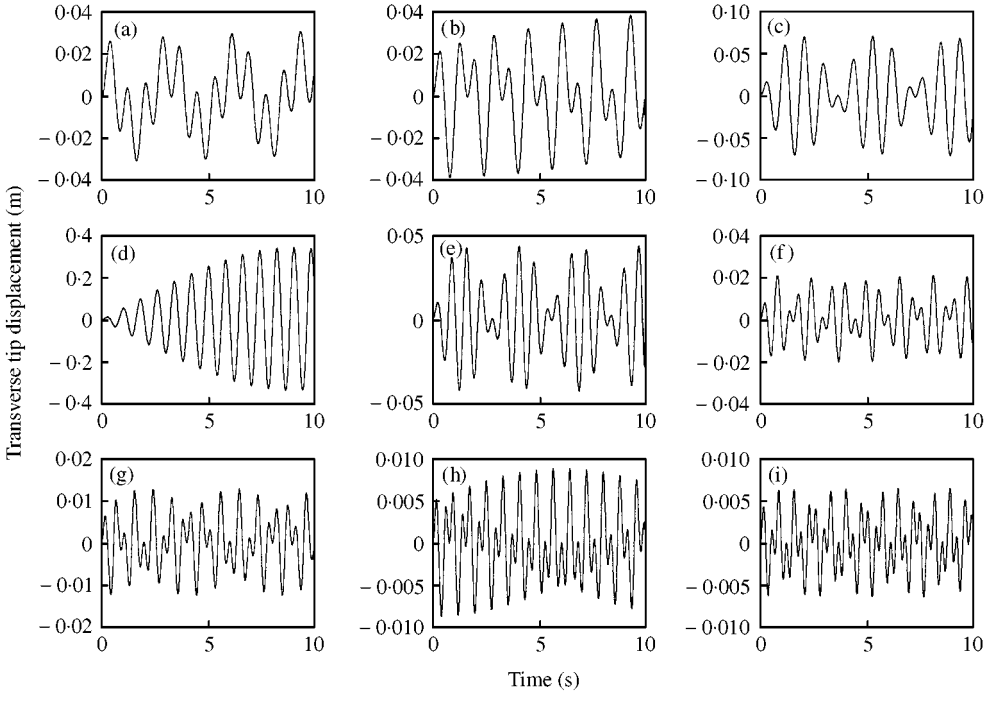

Figure 5. Transverse tip displacement when zero initial conditions are used: (a) $\omega_f = 2$, (b) $\omega_f = 4$, (c) $\omega_f = 6$, (d) $\omega_f = 8$, (e) $\omega_f = 10$, (f) $\omega_f = 12$, (g) $\omega_f = 14$, (h) $\omega_f = 16$, (i) $\omega_f = 18$ rad/s.

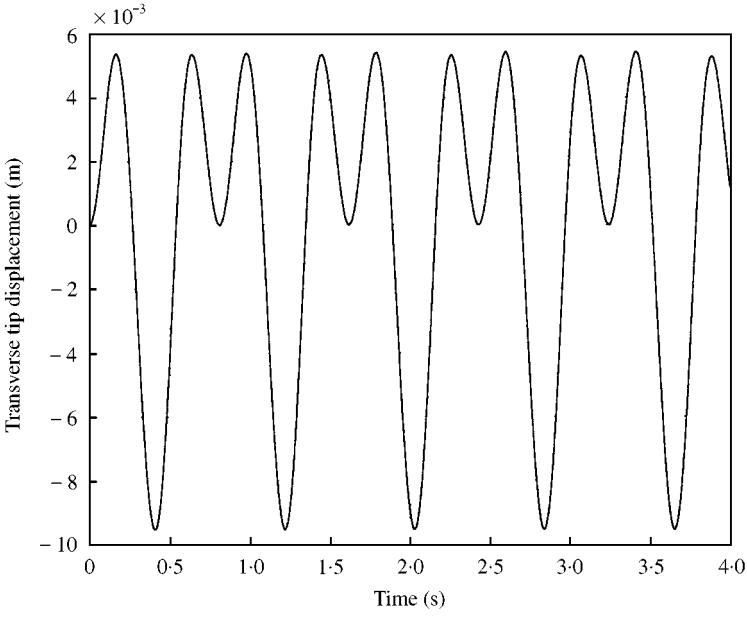

Figure 6. Transverse tip displacement when $\omega_f = 15{\cdot}5$ rad/s.

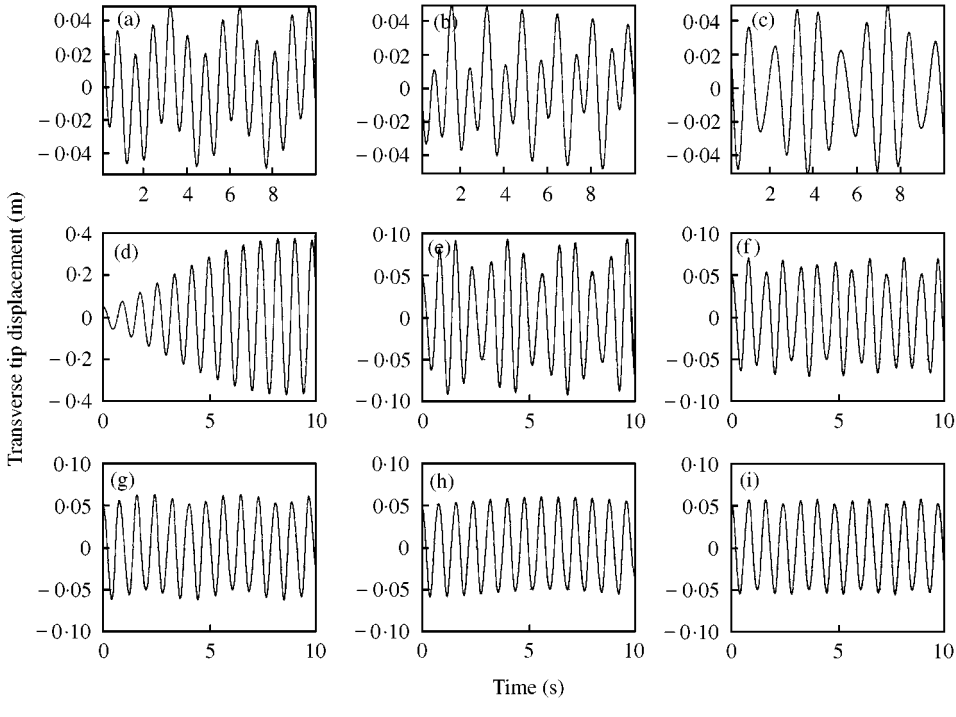

Figure 7. Transverse tip displacement when IC_l is used: (a) $\omega_f = 2$, (b) $\omega_f = 4$, (c) $\omega_f = 6$, (d) $\omega_f = 8$, (e) $\omega_f = 10$, (f) $\omega_f = 12$, (g) $\omega_f = 14$, (h) $\omega_f = 16$, (i) $\omega_f = 18$ rad/s.

3.2. EFFECT OF CURRENT

Figure 8 shows the transverse and axial displacement plots for current velocities of 0·8, 1·2 and 1·6 m/s. Note that the steady state response can be found by solving the equation of motion (1) by setting the time derivatives equal to zero, or

$$-EA_o(u'_{ss} + \tfrac{1}{2}v'^2_{ss})' = p, \tag{23}$$

$$-(EA_o(u'_{ss} + \tfrac{1}{2}v'^2_{ss})v'_{ss})' + (EI_o v''_{ss})'' = f, \tag{24}$$

where

$$p(X,t) = -\rho g A_o + \rho_f g A_f \quad \text{for } 0 < x < d; \; = -\rho g A_o \quad \text{for } d < x < L,$$

$$f(X,t) = C_D \rho_f r_o U_c^2 \quad \text{for } 0 < x < d; \; = 0 \quad \text{for } d < x < L. \tag{25}$$

The subscript *ss* is used for the steady state response. It is not difficult to solve the steady state response numerically. The steady state axial and transverse displacements along the beam are shown in Figure 9. The steady state transverse tip displacements are 0·00154, 0·00346, and 0·00616 m for $U_c = 0{\cdot}08$, 0·12, and 0·16 m/s respectively. The ratio of the transverse tip displacements is 1 : 2·25 : 4. Looking at this ratio, we note that the transverse displacement is proportional to the current velocity squared. This can also be shown by manipulating equations (23) and (24). Therefore, we can write

$$v_{ss}(X) = k_v(X)U_c^2, \tag{26}$$

where k_v is the proportionality constant that depends on the location of the beam. Using the data, $v_{ss}(L) = 0{\cdot}00616$ m when $U_c = 0{\cdot}16$ m/s, the proportionality constant for $X = L$ is found to be 0·241 s^2/m. On the other hand, the steady state axial displacement

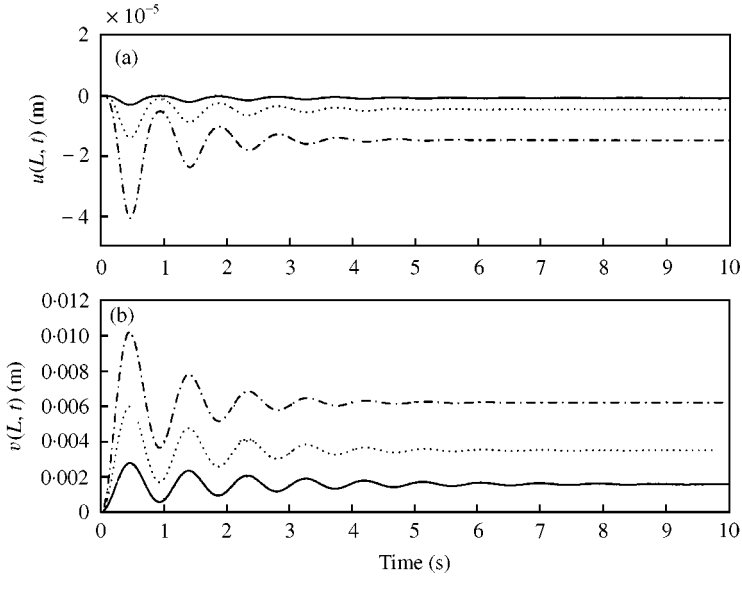

Figure 8. Tip displacements when the beam is subjected to current: ——, $U_c = 0{\cdot}08$; ·····, $U_c = 0{\cdot}12$; –·–·–, $U_c = 0{\cdot}16$ m/s. (a) $u(L, t)$, (b) $v(L, t)$.

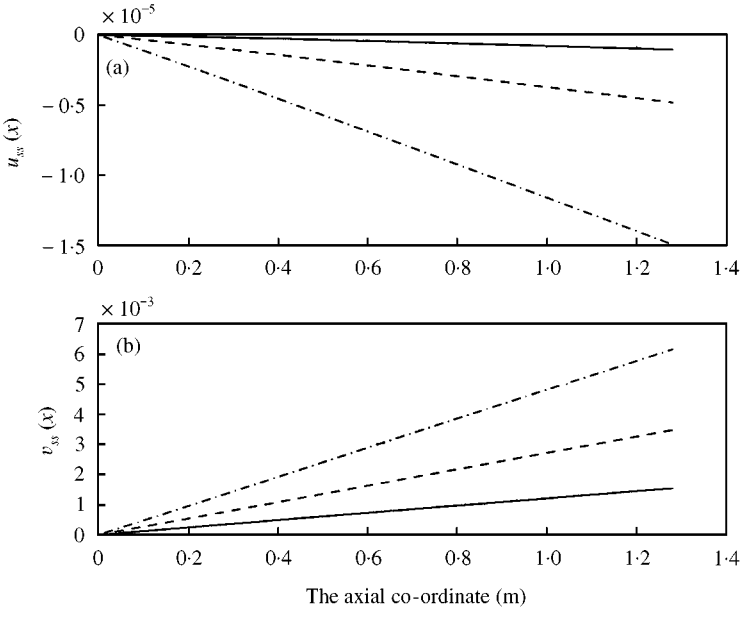

Figure 9. Steady state response when the beam is subjected to current: ——, $U_c = 0{\cdot}08$; – – –, $U_c = 0{\cdot}12$; –·–·–, $U_c = 0{\cdot}16$ m/s. (a) $u_{ss}(L, t)$, (b) $v_{ss}(L, t)$.

is not proportional to the current velocity squared. Instead, it is determined using equation (23).

Now, let us look at the transient response. The maximum transverse displacements are plotted in Figure 10 for the current velocities 0·08, 0·12, 0·16, 0·2, 0·3, and 0·4 m/s. Note that the abscissa is the current velocity squared. The figure shows decreasing slope for increasing current velocities, which means that the maximum transverse tip displacement is proportional to the current velocity to the power slightly less than 2, if it is proportional at all.

As the current velocity increases, the drag increases. This is analogous to increasing the damping coefficient in the linear system. As the damping coefficient increases in the linear system, the damped natural frequency decreases. Therefore, in our case, increasing the current velocity slows the response. Figure 11 shows corresponding physical elongation of the beam for current velocities, 0·08, 0·12, and 0·16 m/s. Surprisingly, the magnitudes are about the same. In fact, the time response looks almost identical. We also notice that the elongations do not decay with time. Now, let us look at the energies of the system. Figures 12 and 13 show the potential and kinetic energies of the system when $U_c = 0{\cdot}08$ m/s. The bending energy and the potential energy stored in the spring approach a non-zero value as time passes. The membrane energy and translational kinetic energy do not decay nor approach steady state value. It was shown in Part 1 that the membrane energy is directly related to the elongation of the beam. It is no surprise that the shapes of the membrane energy and the elongation resemble one another. The non-decaying elongation, membrane energy, and translational kinetic energy indicate that the Morison force is unable to damp the axial motion as shown previously in damped free vibration. However, the axial motion is small compared to the transverse motion so that the steady state analysis in equations (23) and (24) are still valid. The total energy shown in Figure 14 approaches a non-zero value, which is mainly the potential energy stored in the system.

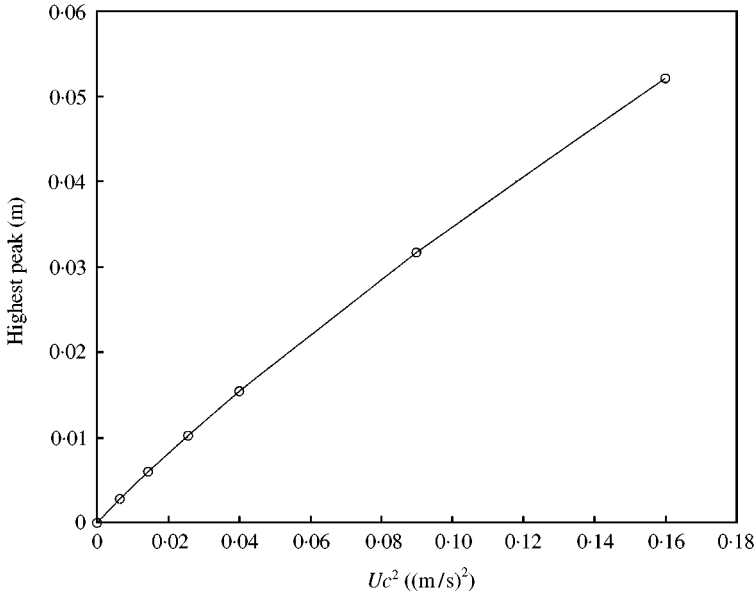

Figure 10. Peak amplitude of tip displacement.

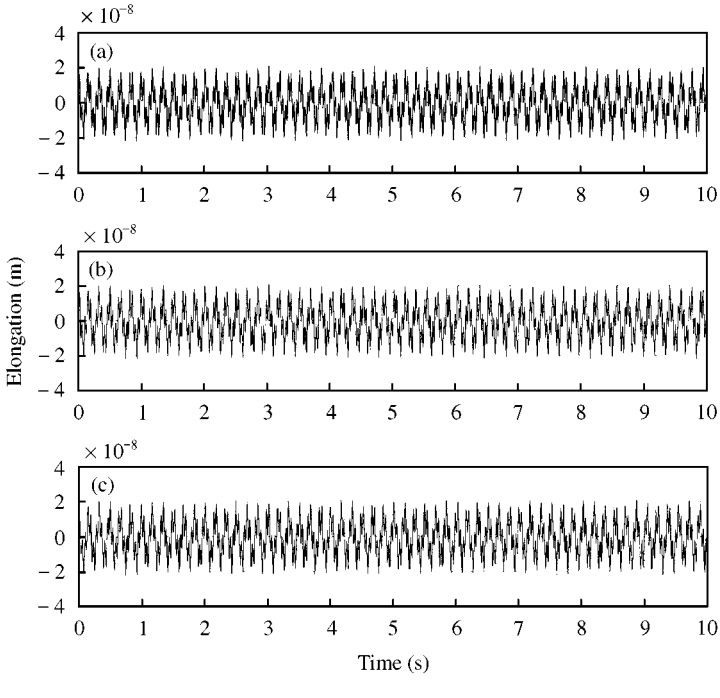

Figure 11. Elongation of the beam: (a) $U_c = 0{\cdot}08$, (b) $U_c = 0{\cdot}12$, (c) $U_c = 0{\cdot}16$ m/s.

3.3. EFFECT OF RANDOM WAVES

The significant wave height is varied such that the peak angular frequency is varied from 2 to 18 rad/s at 2 rad/s interval. That is, the corresponding significant wave heights,

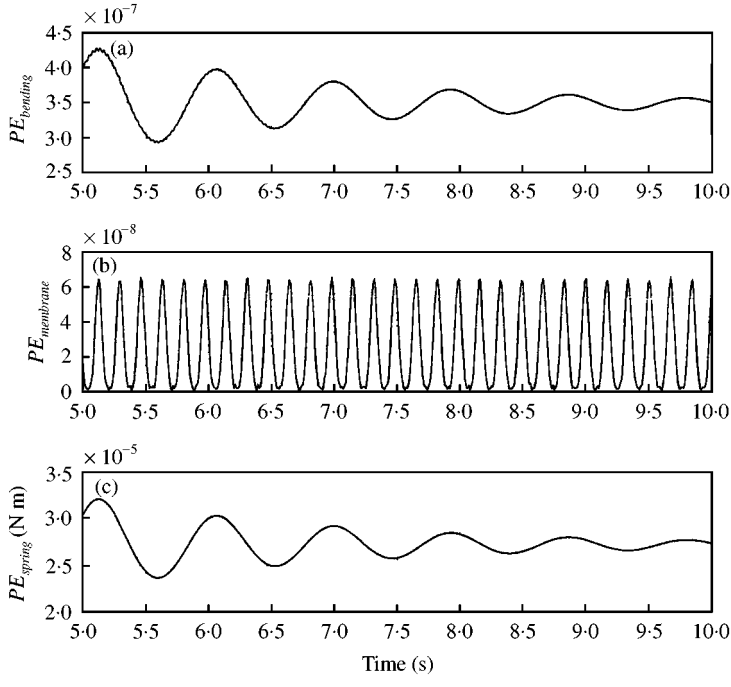

Figure 12. Potential energy for $U_c = 0{\cdot}08$ m/s: (a) $PE_{bending}$, (b) $PE_{membrane}$, (c) PE_{spring}.

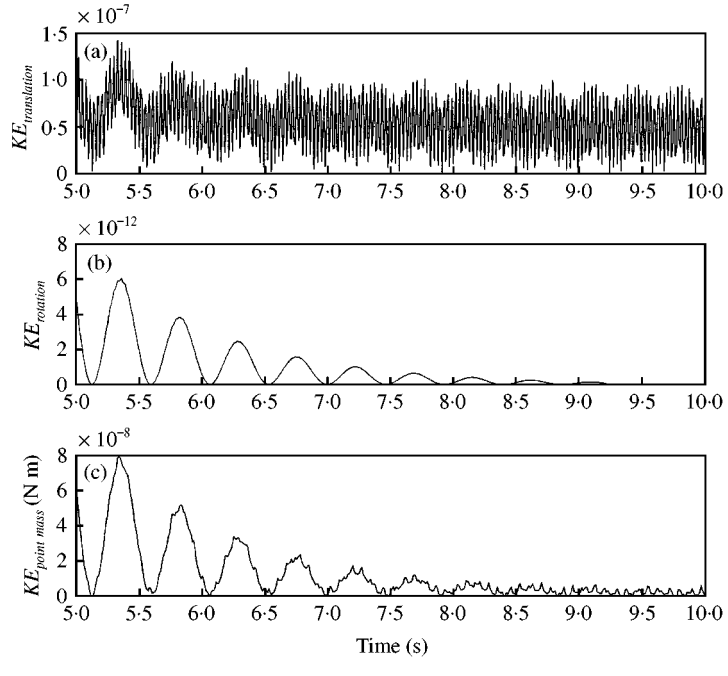

Figure 13. Kinetic energy for $U_c = 0{\cdot}08$ m/s: (a) $KE_{translation}$, (b) $KE_{rotation}$, (c) $KE_{point\ mass}$.

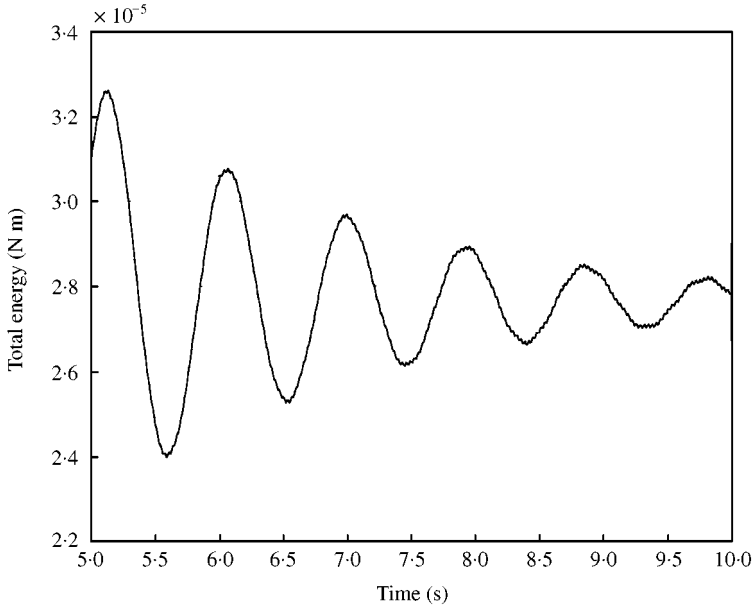

Figure 14. Total energy for $U_c = 0{\cdot}08$ m/s.

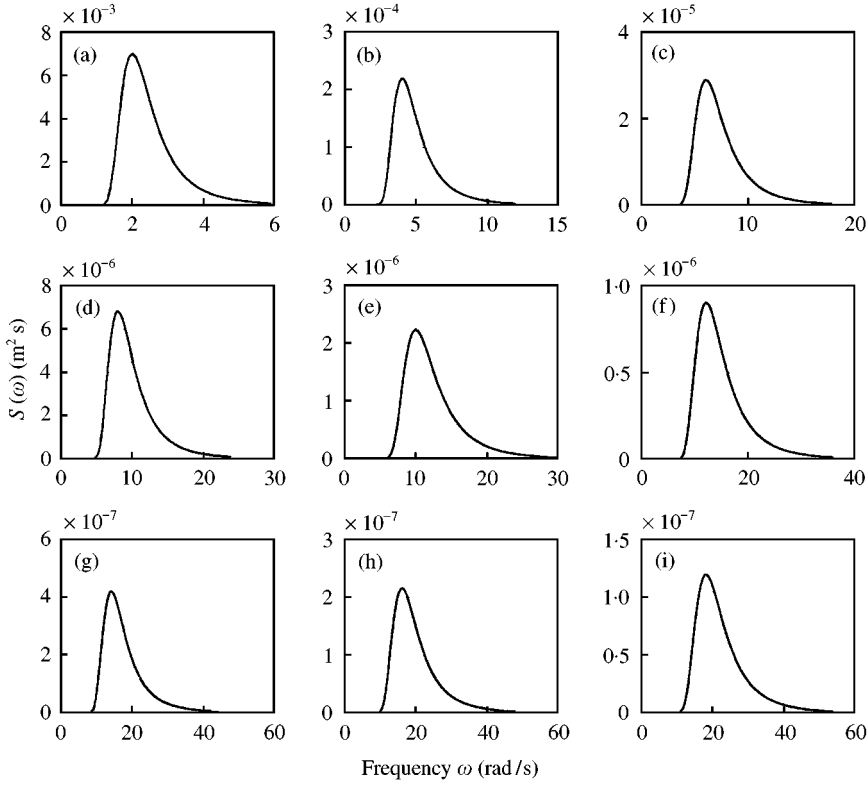

Figure 15. Pierson–Moskowitz spectrum: (a) $\omega_{peak} = 2$, $H_s = 0{\cdot}3957$; (b) 4, 0·0989; (c) 6, 0·044; (d) 8, 0·0247; (e) 10, 0·0158; (f) 12, 0·011; (g) 14, 0·0081; (h) 16, 0·0062; (i) 18 rad/s, 0·0049.

from equation (16) are 0·3957, 0·0989, 0·0440, 0·0247, 0·0158, 0·0110, 0·0081, 0·0062, and 0·0049 m. The Pierson–Moskowitz spectra are plotted in Figure 15. In the laboratory setting, a significant wave height of 0·1 m may be plausible. Note that the magnitude of power spectral density decreases with decreasing significant wave height or increasing peak frequency. For $\omega_{peak} = 2$ rad/s, the wave heights, $\eta(y = 0, t)$ and $\eta(y, t = 0)$, are plotted in Figures 16(a) and 16(b). The corresponding horizontal and vertical wave velocities at $t = 0$

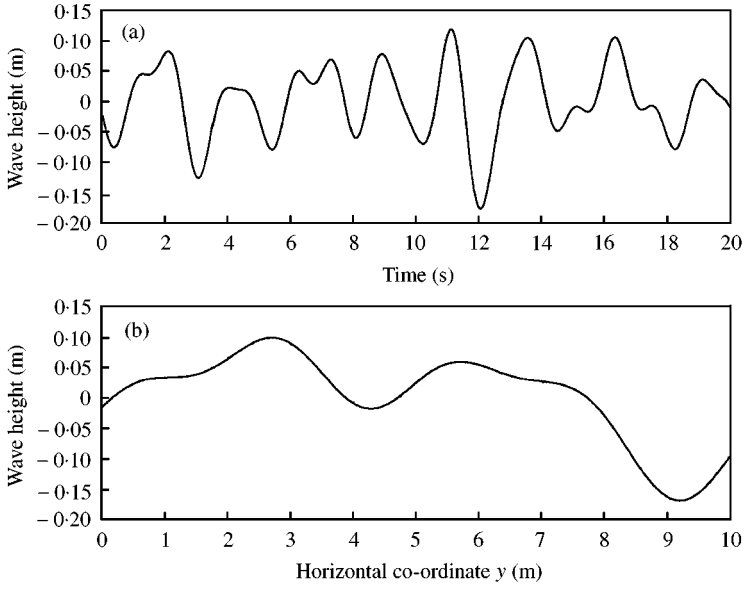

Figure 16. Wave height for $\omega_{peak} = 2$ rad/s: (a) wave height versus time, (b) wave height versus horizontal co-ordinate.

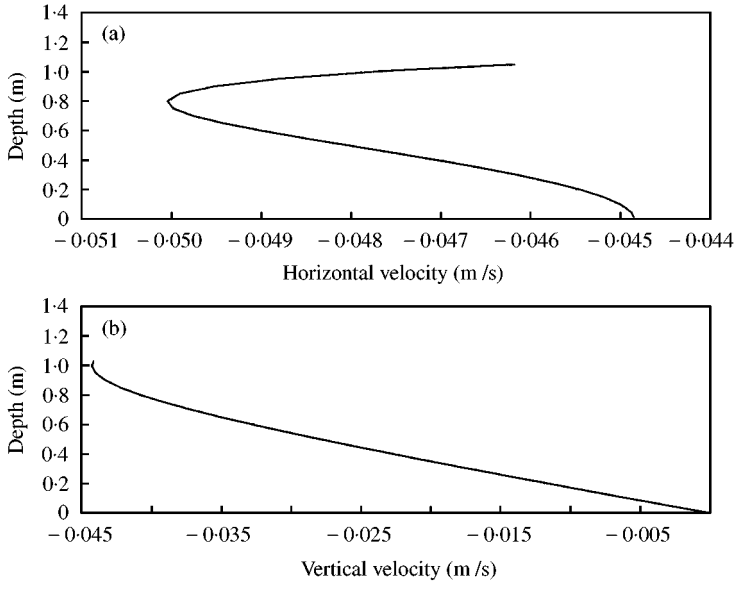

Figure 17. Wave velocities for $\omega_{peak} = 2$ rad/s: (a) horizontal velocity, (b) vertical velocity.

and $y = 0$ are plotted as a function of depth in Figure 17(a) and 17(b). For $\omega_{peak} = 18$ rad/s, similar plots are shown in Figures 18 and 19. Note that the magnitude of wave heights and velocities also decreased with increasing peak frequency.

The transverse displacements are plotted in Figure 20 when zero initial conditions are used. We observe a beating phenomenon in many of the responses. They are not well defined as in the linear case. The magnitude of the response generally decreased with

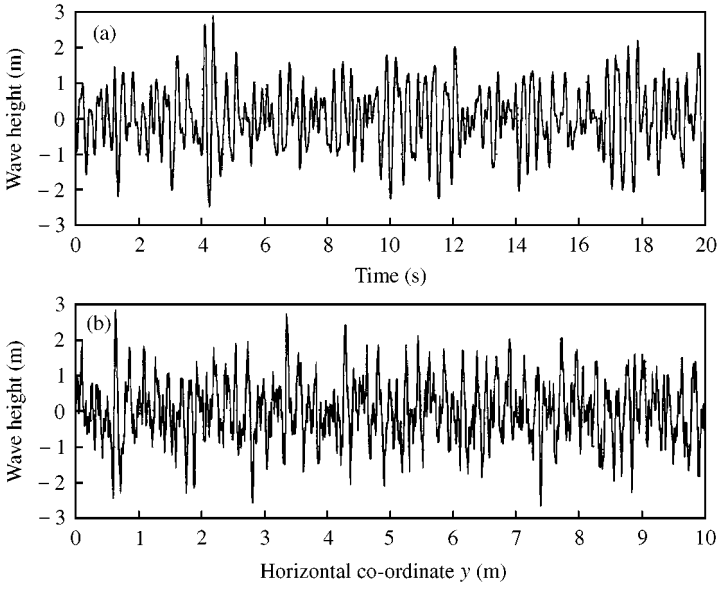

Figure 18. Wave height for $\omega_{peak} = 18$ rad/s: (a) wave height versus time, (b) wave height versus horizontal co-ordinate.

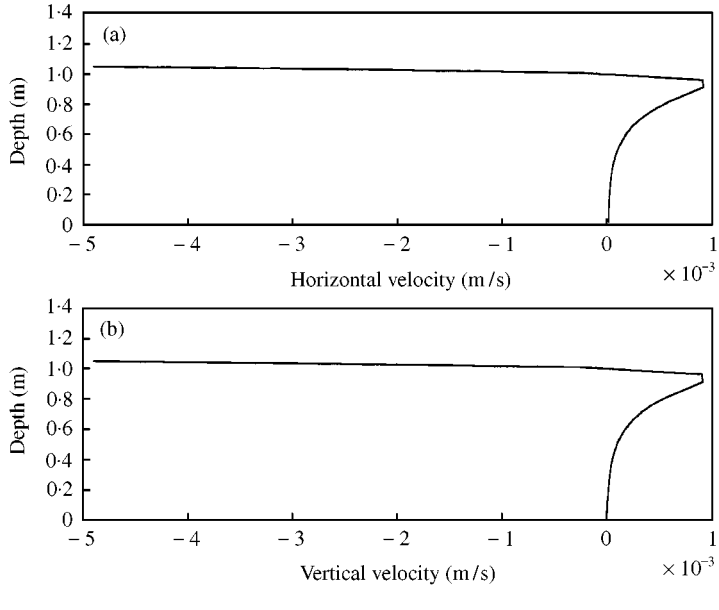

Figure 19. Wave velocities for $\omega_{peak} = 18$ rad/s: (a) horizontal velocity, (b) vertical velocity.

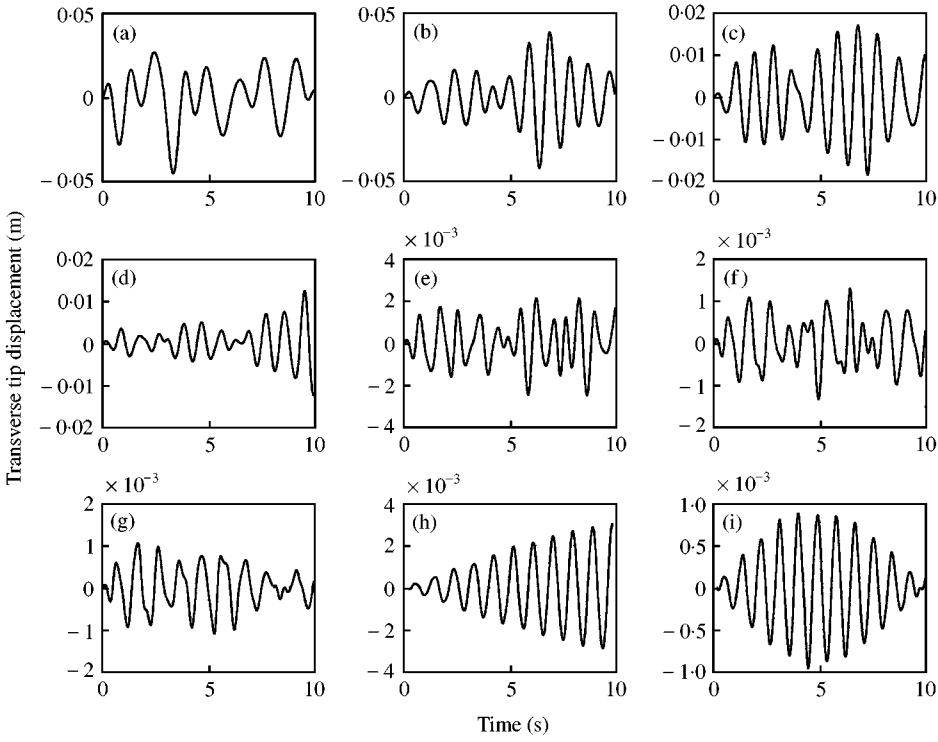

Figure 20. Transverse tip displacement when zero initial conditions are used: (a) $\omega_{peak} = 2$, (b) $\omega_{peak} = 4$, (c) $\omega_{peak} = 6$, (d) $\omega_{peak} = 8$, (e) $\omega_{peak} = 10$, (f) $\omega_{peak} = 12$, (g) $\omega_{peak} = 14$, (h) $\omega_{peak} = 16$, (i) $\omega_{peak} = 18$ rad/s.

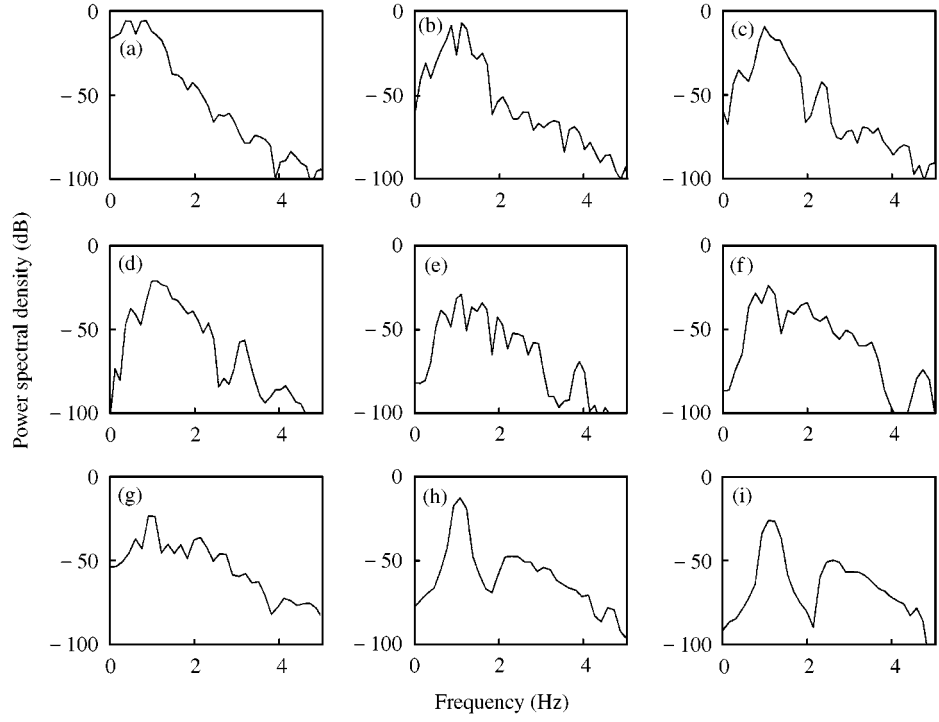

Figure 21. Power spectral density plots for the transverse tip displacements when zero initial conditions are used: (a) $\omega_{peak} = 2$, (b) $\omega_{peak} = 4$, (c) $\omega_{peak} = 6$, (d) $\omega_{peak} = 8$, (e) $\omega_{peak} = 10$, (f) $\omega_{peak} = 12$, (g) $\omega_{peak} = 14$, (h) $\omega_{peak} = 16$, (i) $\omega_{peak} = 18$ rad/s.

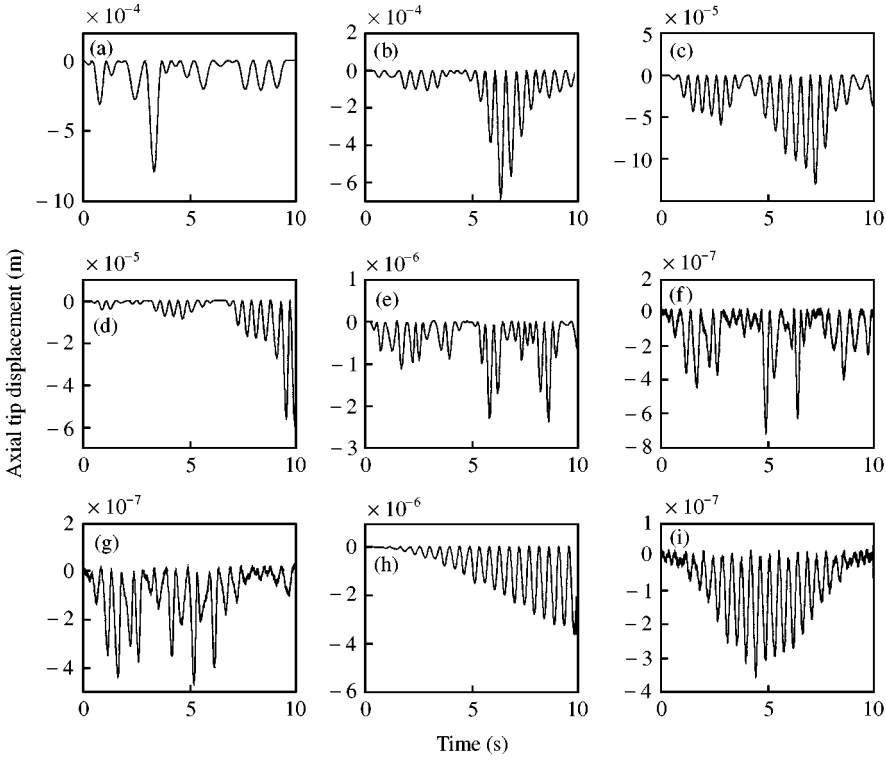

Figure 22. Axial tip displacement when zero initial conditions are used: (a) $\omega_{peak} = 2$, (b) $\omega_{peak} = 4$, (c) $\omega_{peak} = 6$, (d) $\omega_{peak} = 8$, (e) $\omega_{peak} = 10$, (f) $\omega_{peak} = 12$, (g) $\omega_{peak} = 14$, (h) $\omega_{peak} = 16$, (i) $\omega_{peak} = 18$ rad/s.

increasing peak frequency. This is because the wave velocities decrease with the peak frequency. Figure 21 shows power spectral density plots for the transverse tip displacements. The data points are sampled at 0·0005 s intervals. We obtain a consistent peak at about 1 Hz. This frequency must be the damped natural frequency of the system. Note that it is different from the damped natural frequency obtained in still water or the damped natural frequency when there is only current. This is because the damping force is different in each case. Figure 22 shows the corresponding axial displacements. The general shape of the axial response is similar to those shown in Part 1: the fundamental frequency of the axial motion is twice that of the transverse motion, and the maximum of each peak of the dominant axial motion is the same, so that the dominant axial motion seems to have a ceiling. It was shown in Part 1 that this is due to the geometry of the system. Figure 23 shows the elongation of the beam as a function of time. The amplitude in most cases are about 2×10^{-8} m. When $\omega_{peak} = 2$ and 4 rad/s, we observe spurious peaks in elongations. Figures 24 and 25 show the potential and kinetic energies when $\omega_{peak} = 10$ rad/s. The energies have some of the same characteristics observed in the free vibration: shape of elongation resembles the shape of the membrane energy, the potential energies and the kinetic energies are in phase, the potential energies and the kinetic energies are 180° out of phase. Figure 26 shows the total energy of the system. It shows that the total energy does not decay. Instead, it fluctuates randomly due to the random forcing.

The transverse displacements are plotted in Figure 27, where the initial displacements in equation (21) are used. The power spectral densities are plotted in Figure 28. The dominant

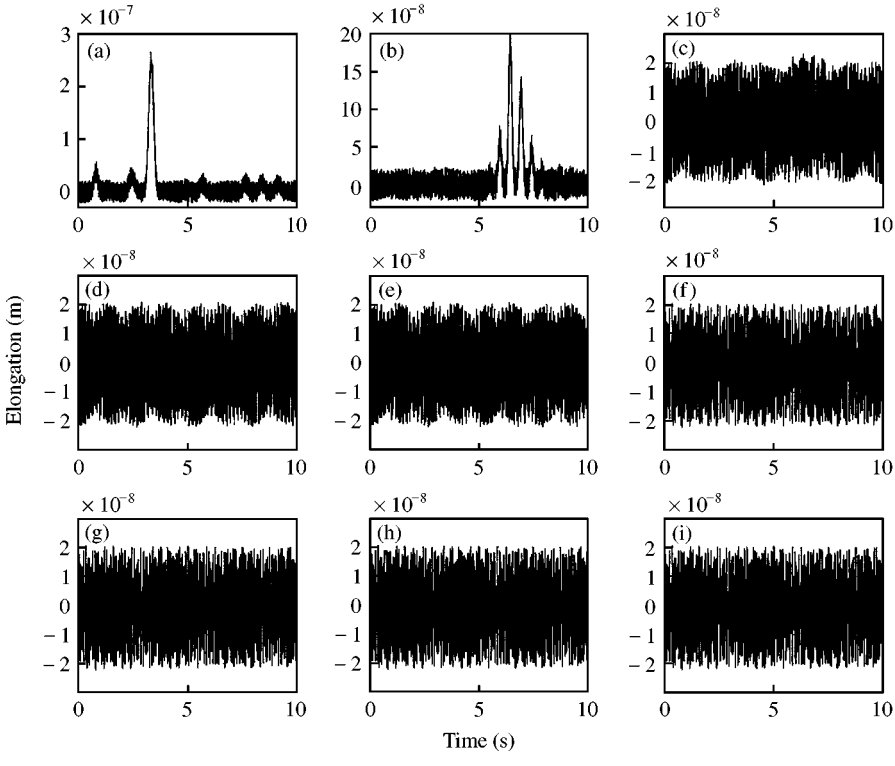

Figure 23. Elongation when zero initial conditions are used: (a) $\omega_{peak} = 2$, (b) $\omega_{peak} = 4$, (c) $\omega_{peak} = 6$, (d) $\omega_{peak} = 8$, (e) $\omega_{peak} = 10$, (f) $\omega_{peak} = 12$, (g) $\omega_{peak} = 14$, (h) $\omega_{peak} = 16$, (i) $\omega_{peak} = 18$ rad/s.

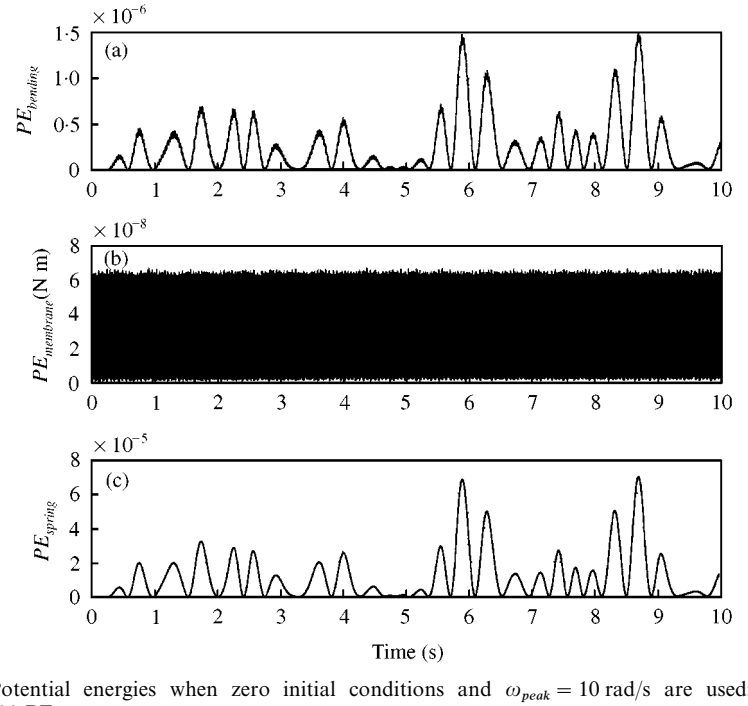

Figure 24. Potential energies when zero initial conditions and $\omega_{peak} = 10$ rad/s are used: (a) $PE_{bending}$, (b) $PE_{membrane}$, (c) PE_{spring}.

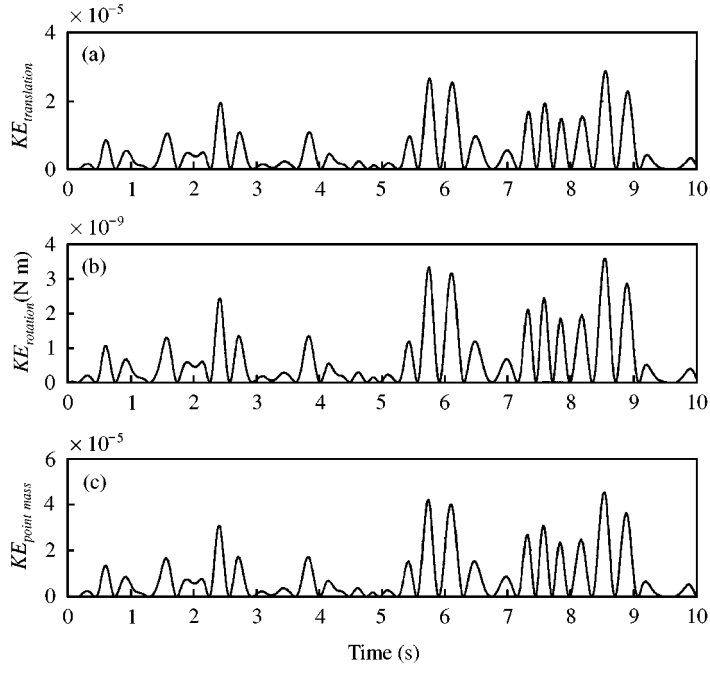

Figure 25. Kinetic energies when zero initial conditions and $\omega_{peak} = 10$ rad/s are used: (a) $KE_{translation}$, (b) $KE_{rotation}$, (c) $KE_{point\ mass}$.

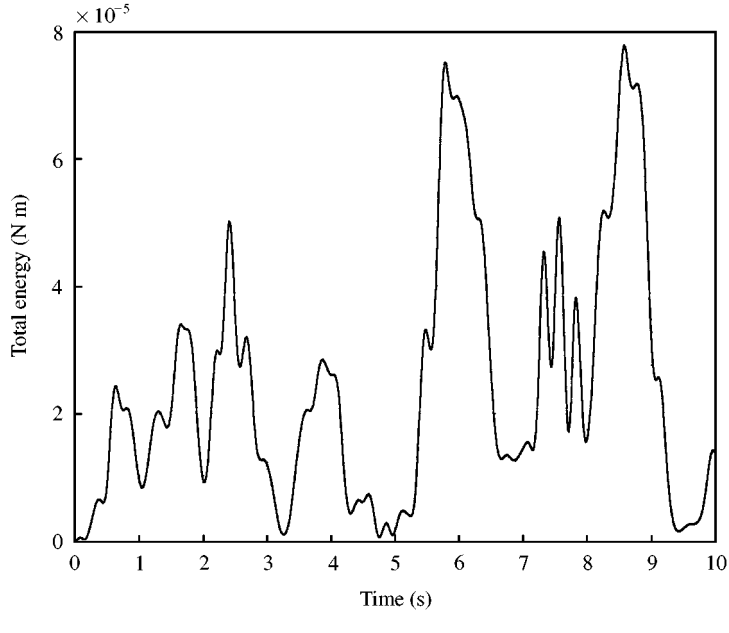

Figure 26. Total energy when zero initial conditions and $\omega_{peak} = 10$ rad/s are used.

frequency of all responses is the damped natural frequency at about 1 Hz. We observe subharmonic resonances in Figures 29(c)–(i). Note that we observe that the subharmonic resonance occurs for a relatively wide range of the peak frequency, ω_{peak}. This is due to the fact that the transverse force is random and the forcing frequency is spread out around

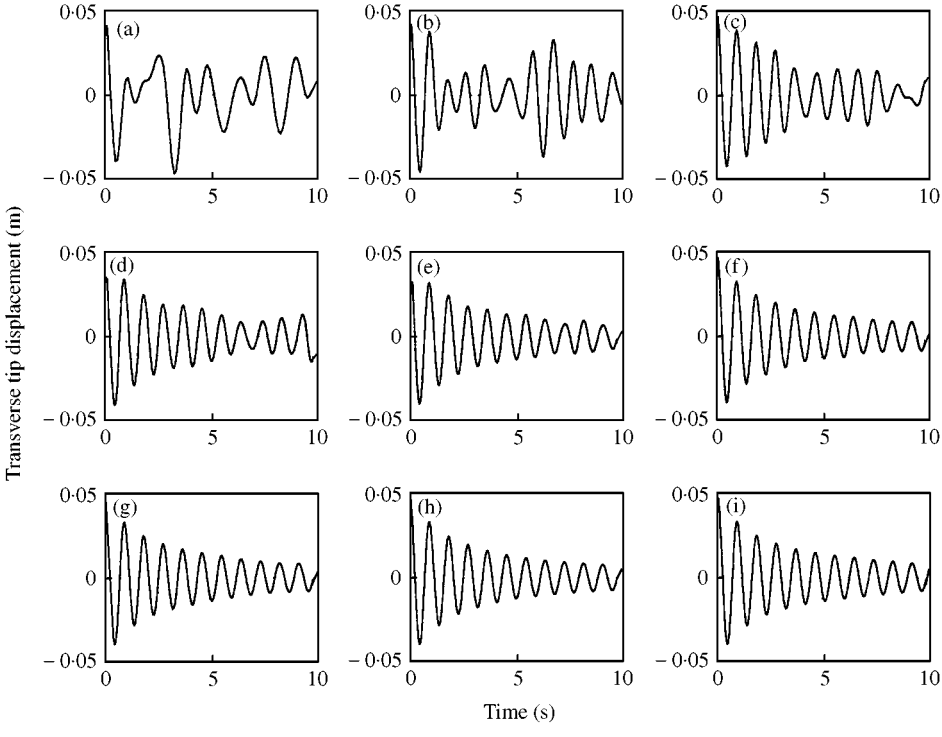

Figure 27. Transverse tip displacement when non-zero initial conditions are used: (a) $\omega_{peak} = 2$, (b) $\omega_{peak} = 4$, (c) $\omega_{peak} = 6$, (d) $\omega_{peak} = 8$, (e) $\omega_{peak} = 10$, (f) $\omega_{peak} = 12$, (g) $\omega_{peak} = 14$, (h) $\omega_{peak} = 16$, (i) $\omega_{peak} = 18$ rad/s.

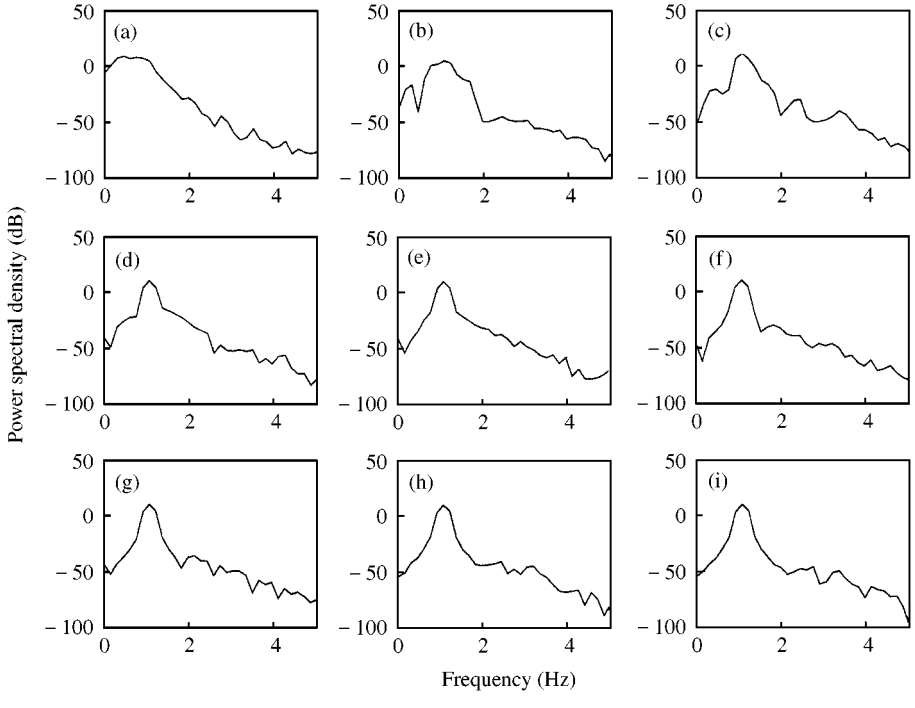

Figure 28. Power spectral density plots for the transverse tip displacements when non-zero initial conditions are used: (a) $\omega_{peak} = 2$, (b) $\omega_{peak} = 4$, (c) $\omega_{peak} = 6$, (d) $\omega_{peak} = 8$, (e) $\omega_{peak} = 10$, (f) $\omega_{peak} = 12$, (g) $\omega_{peak} = 14$, (h) $\omega_{peak} = 16$, (i) $\omega_{peak} = 18$ rad/s.

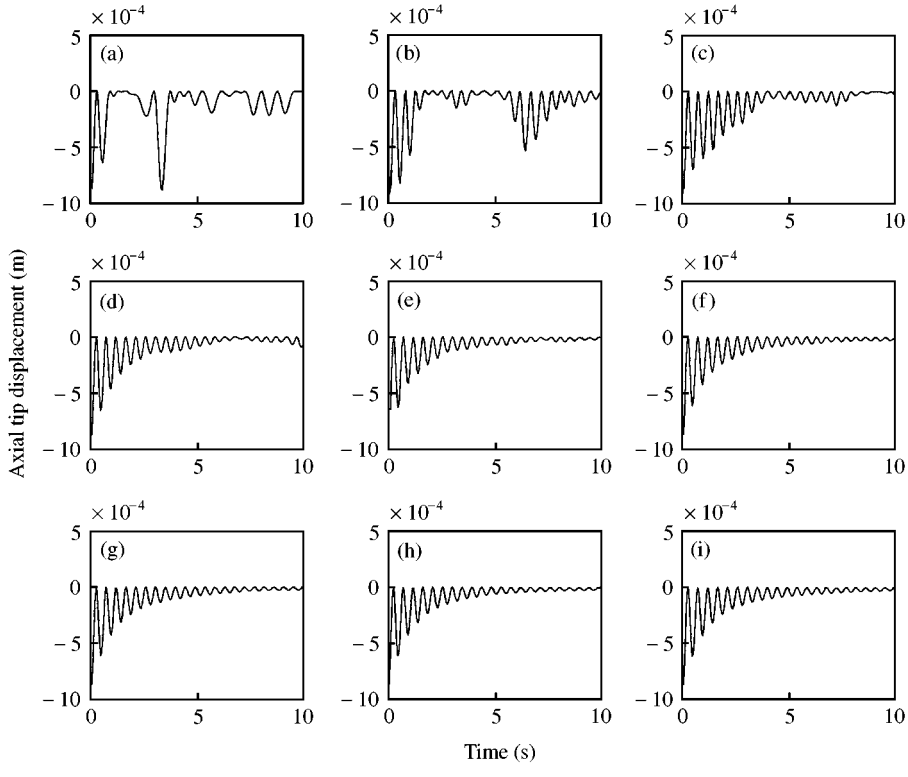

Figure 29. Axial tip displacement when non-zero initial conditions are used: (a) $\omega_{peak} = 2$, (b) $\omega_{peak} = 4$, (c) $\omega_{peak} = 6$, (d) $\omega_{peak} = 8$, (e) $\omega_{peak} = 10$, (f) $\omega_{peak} = 12$, (g) $\omega_{peak} = 14$, (h) $\omega_{peak} = 16$, (i) $\omega_{peak} = 18$ rad/s.

ω_{peak}. Figure 30 shows the elongation of the beam. The amplitudes are about 10^{-6} m for all cases. It should be noted that the responses look similar to the ones we have seen in the damped free vibration where water was still. That is, the damping effect in the Morison force must be dominant when non-zero initial conditions are applied. Figures 31 and 32 show potential and kinetic energies of the system when $\omega_{peak} = 10$ rad/s. Figure 33 shows the total energy of the system. These plots show that the energies decay with time due to damping. After the transient response dies out, we expect to see similar random patterns as when zero initial conditions were used.

4. SUMMARY AND CONCLUSIONS

As a continuation of Part 1, we studied the forced response of beam under the environmental loading due to current and waves. The fluid force was modelled by the Morison equation, and the waves were modelled as random using the Pierson–Moskowitz spectrum and Airy linear wave theory.

When the harmonic force was applied, we observed the subharmonic resonance for the forcing frequency near the natural frequency.

When only current was present, the transverse offset from the vertical at the tip was proportional to the current velocity squared. The magnitude of highest transverse peak in

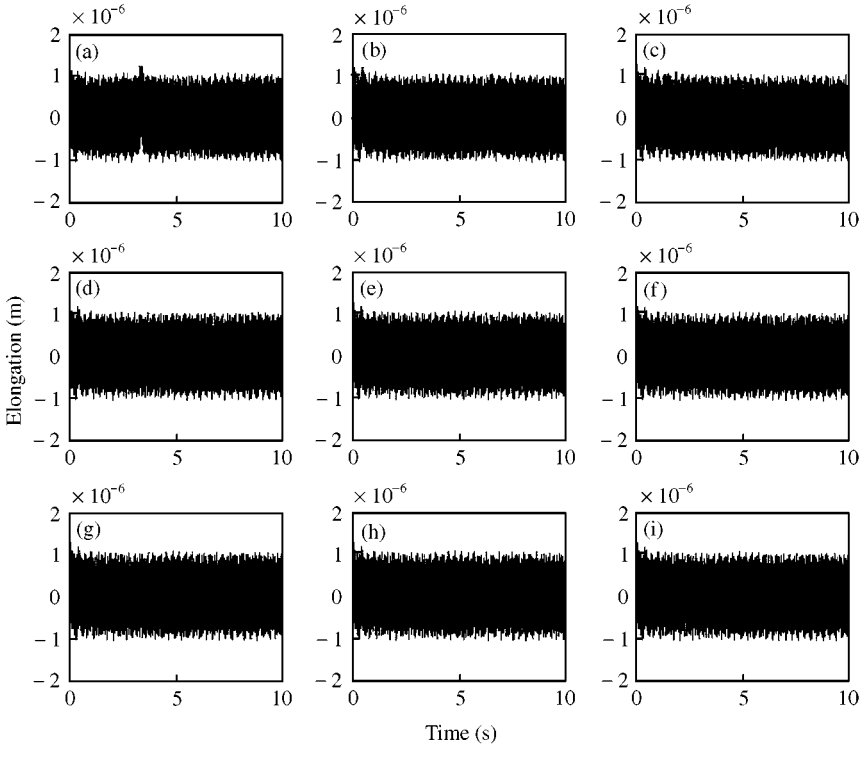

Figure 30. Elongation when non-zero initial conditions are used: (a) $\omega_{peak} = 2$, (b) $\omega_{peak} = 4$, (c) $\omega_{peak} = 6$, (d) $\omega_{peak} = 8$, (e) $\omega_{peak} = 10$, (f) $\omega_{peak} = 12$, (g) $\omega_{peak} = 14$, (h) $\omega_{peak} = 16$, (i) $\omega_{peak} = 18$ rad/s.

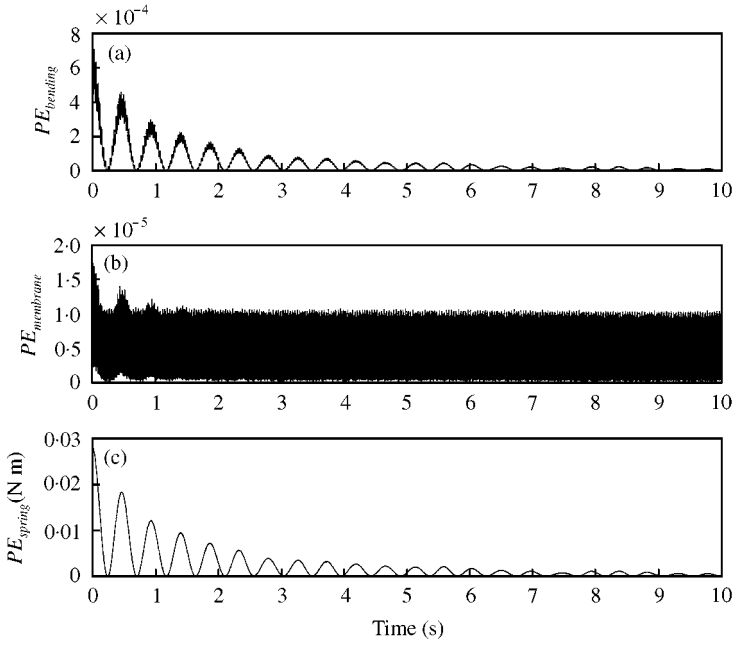

Figure 31. Potential energies when non-zero initial conditions and $\omega_{peak} = 10$ rad/s are used: (a) $PE_{bending}$, (b) $PE_{membrane}$, (c) PE_{spring}.

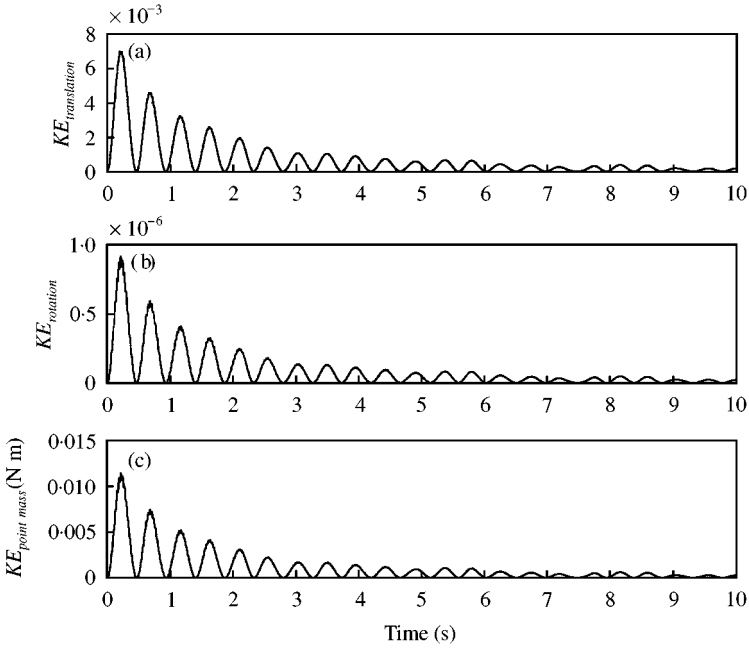

Figure 32. Kinetic energies when non-zero initial conditions and $\omega_{peak} = 10$ rad/s are used: (a) $KE_{translation}$, (b) $KE_{rotation}$, (c) $KE_{point\ mass}$.

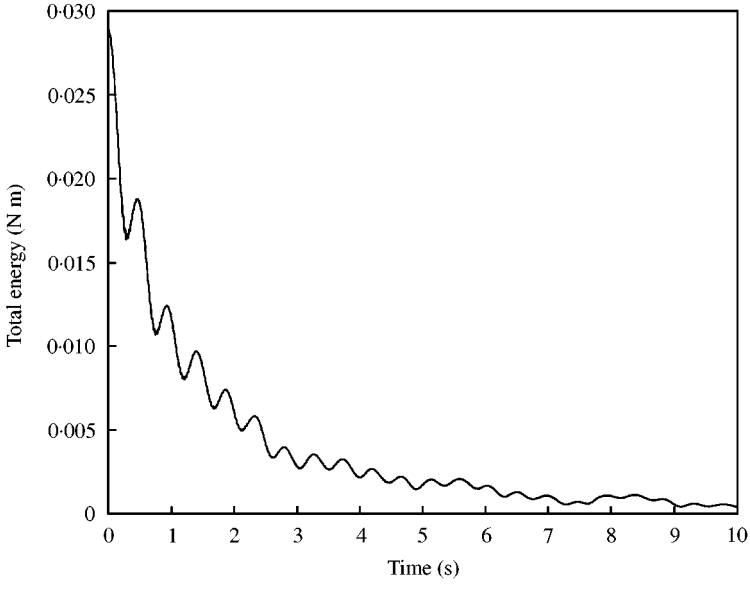

Figure 33. Total energy when non-zero initial conditions are used.

the transient response did not quite follow the same rule. Instead, the magnitudes were slightly less than what was predicted by the current-velocity-squared rule.

When the random fluid force was applied, the subharmonic resonance was not observed when zero initial conditions were used. When the non-zero initial conditions were used, the

subharmonic resonance of order 1/2 was observed for a wide range of significant wave heights. In all cases, the axial displacement had the same characteristics as in the free vibration case. The dominant frequency was twice that of the transverse vibration, and the maximum of each peak of the dominant axial motion is the same. The amplitude of elongation for various peak frequencies were close to each other for each initial condition.

When zero initial conditions were used, we observed spurious peaks in elongations for $\omega_{peak} = 2$ and 4 rad/s. The total energy of the system varied randomly with time. When non-zero initial conditions were used, we saw uniform elongations for all cases. The responses look similar to those for the damped free cases. The total energy of the system decayed with time. However, we expect that the random effect may become more pronounced after the transient response dies out.

ACKNOWLEDGMENTS

This work was supported by the Office of Naval Research Grant No. N00014-97-1-0017. We would like to thank our program manager Dr. Thomas Swean for his interest and financial support. The first author also would like to thank Dr. Patrick Bar-Avi and Dr. Ronald Adrezin, his predecessors, for their previous works [12, 13] and early assistance. The authors are pleased to acknowledge the continued collaboration with their colleague, Professor Timothy Wei.

REFERENCES

1. S. HAN and H. BENAROYA 2000 *Journal of Sound and Vibration* **237**, 837–873. Non-linear coupled transverse and axial vibration of a compliant structure, part I: Formulation and free vibration.
2. J. R. MORISON, M. P. O'BRIEN, J. W. JOHNSON and S. A. SCHAAF 1950 *Petroleum Transaction, AIME* **189**, 149–157. The force exerted by surface waves on piles.
3. M. ISAACSON 1988 *Canadian Journal of Civil Engineering* **15**, 937–947. Wave and current forces on fixed offshore structures.
4. S. CHAKRABARTI 1987 *Hydrodynamics of Offshore Structures*. Southampton, Great Britain: Computational Mechanics Publications, Inc.
5. H. SVERDRUP and W. MUNK 1947 *Wind, Sea, and Swell: Theory and Relations for Forecasting*. U.S. Navy Hydrographic Office, Publication No. 601.
6. H. BENAROYA 1998 *Mechanical Vibration*. Upper Saddle River, NJ: Prentice-Hall Inc.
7. L. BORGMAN 1969 *Journal of the Waterway and Harbors Division* **95**, 557–583. Ocean wave simulation for engineering design.
8. R. PANTON 1996 *Incompressible Flow*. New York: Wiley.
9. J. STOKER 1950 *Nonlinear Vibrations in Mechanical and Electrical Systems* (*Wiley Classic Library*). New York: Wiley.
10. N. MINORSKY 1962 *Nonlinear oscillations*. Malabar, FL: Robert E. Krieger Publishing Company, Inc.
11. B. MUGA and J. WILSON 1970 *Dynamics Analysis of Ocean Structures*. New York: Plenum Press.
12. R. ADREZIN 1997 *The nonlinear stochastic dynamics of tension leg platforms*, Ph.D. Thesis. Rutgers, the State University of New Jersey.
13. P. BAR-AVI 1996 *Dynamic Response of an Offshore Articulated Tower, Ph.D. Thesis, Rutgers, the State University of New Jersey*.